Design loading optimization of a horizontal axis turbine with lifting line and panel methods

Emanuele Quarona

emanuelequarona@gmail.com

Instituto Superior Técnico, Universidade de Lisboa, Portugal

October, 2019

ABSTRACT

A method to optimize the circulation distribution for wind turbines is herewith presented. Through the lifting line method the optimization is done using the wake geometries obtained with the panel method analysis. After two iterations of the outer cycle, the convergence of the power coefficient is obtained and the final design of the blades is done. The wake geometries and the pitch distributions proving the consistency of the method are discussed and they prove that the wake geometry obtained fold in the downstream direction, unlike the works conducted in the previous years. A viscous situation is also assessed and the results in this case are in good agreement with the literature, confirming once again that the optimization procedure used is accurate and reliable.

KEYWORDS: Lifting line theory, Panel method, Wind turbine, Wake alignment.

1. INTRODUCTION

Since the end of the 19th century, the improvements in the aerodynamics and fluid mechanics fields have been remarkable. The formulation of the lifting line theory surely gave fundamental insights for the development of many technologies. It was Frederick W. Lanchester that in 1907 set the basics for the lifting line theory (Lanchester, 1907). From this point on, many improvements were done to the theory according to the applications of it, in fact the lifting line has been used for the design and analysis of many lifting surfaces like wings, propellers and ultimately horizontal axis wind turbines.

As a matter of fact, the lifting line theory is not accurate enough, and over the century new computational based theories such as the panel methods (1970s) were developed. With this model it is possible to take into account the geometry of the blades and it is possible to obtain a more accurate description of how the fluid behaves along the blade, at the trailing edge and at the wake region. (Erickson, 1990)

At the MARETEC/IST lot of work has being done on the design optimization of propellers and wind turbines: Duarte & Fãlcao de Campos (1997) developed a lifting line code that was then improved by Falcão de Campos (2007) in his work on optimization of a marine current turbine. Machado (2010) then added the effect of the hub and Caldeira (2014) added the viscous effects. Melo (2016) using the numerical approach by Baltazar, Falcão de Campos, & Bosschers (2012), implemented the analysis code for wind turbines adding a wake alignment scheme by discretizing it and Sousa (2018) succeeded to perform the optimization procedure adjusting the analysis code by Melo implementing the Lagrange multiplier method instead of the classical one so far used. At the same time panel method codes were also developed for propellers and later Baltazar & Falcão de Campos (2011) adapted a code to the case of marine current turbines. For what regards the case of the wind turbines the panel method has not been widely used and that is why the focus of this thesis is the combination of the lifting line method with the panel method for a horizontal axis wind turbine in order to obtain a more accurate wake geometry and therefore an improved design of the blades.

As the energy transition is happening, the importance of the wind industry worldwide is clear and that is the reason why the improvements of the optimization, design and analysis computational codes of the wind turbines are so important for the sustainability of our planet, both from the economical and environmental point of view.

2. THEORY

Lifting line theory

The theory uses the circulation concept and the Kutta-Joukowski theorem:

$$\vec{L} = -\rho\overrightarrow{V_\infty} \times \vec{\Gamma}, \tag{1}$$

where ρ and V_∞ are respectively the air density and the velocity far upstream and $\Gamma = \oint \vec{V} \cdot \overrightarrow{ds}$ is the circulation

vector. With this formula the unknown becomes the circulation function instead of the lift force one, in fact the span-wise change in lift is equivalent to a span-wise change of circulation. (Anderson, 2001)

Any span-wise change in lift can be modelled as the shedding of a vortex filament down the flow, behind the wing and it is usually proportional to the pressure difference between the upper and the lower surface of the blade. At the tip of the blade the difference becomes zero and the secondary flow appears: the fluid tends to move around the tip, going up to the low-pressure surface of the blade. The circulation distribution and consequently the lift will strongly depend on the pressure distribution, resulting zero at the tip.

2.1 Velocity field

Consider the rotor of a horizontal axis wind turbine with radius R and hub radius r_h and Z blades symmetrically placed around the hub. Assume the rotor rotating with an angular velocity ω in a uniform flow velocity field U, aligned with the rotation axis. It is possible to define a cartesian coordinate system (x, y, z) and a cylindrical coordinate system (x, r, θ) in a reference frame rotating with the turbine rotor. The relative velocity field is given by $\vec{V_\infty} = \vec{U} - \vec{\omega} \times \vec{r}$,as shown in Figure 1.

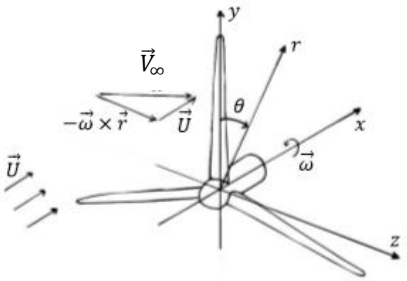

Figure 1: Adopted coordinate system and inflow velocity field, $Z = 3$ (Melo, 2016).

In the lifting line model, every blade is represented by a radial bound vortex, expanding from the root of the blade to the tip. Due to the variation of circulation along the blade, trailing vortices are shed from each lifting line, generating a vortex sheet.

In Figure 2 it is possible to see the vortex system for one of the three blades.

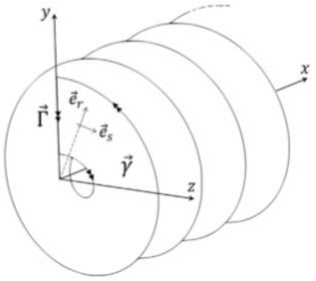

Figure 2: Lifting line and corresponding vortex sheet(Melo, 2016).

It is important to remark that in the force-free vortex wake, the vortex filaments must be aligned with the local velocity field giving the product $\vec{\gamma} \times \vec{V} = 0$.

If now one wants to consider the effect of the bound and the trailing vortices, the velocity induced by the lifting line k and its sheet of trailing vortices can be computed in any point in space by the Biot Savart law:

$$\vec{v}_k(x, y, z) = \frac{1}{4\pi} \int_{L_k} \frac{\vec{\Gamma} \times \vec{R}}{R^3} dl + \frac{1}{4\pi} \int_{S_k} \frac{\vec{\gamma} \times \vec{R}}{R^3} dS, \qquad (2)$$

where $\vec{R}$ is the vector going from the integration point to the point (x, y, z) where the computation of the induced velocities is being done.

The total induced velocities are obtained by the sum of the Z blades contributions:

$$\vec{v}(x, y, z) = \sum_{k=1}^{Z} \vec{v}_k(x, y, z) \ , \qquad (3)$$

At this point, summing up the total induced velocities and the undisturbed velocity field component it is possible to get the velocity field in cylindrical coordinates:

$$\vec{V}(x, r, \theta) = (U - v_a, v_r, \omega r + v_t). \qquad (4)$$

2.2 Angles, forces and power coefficient

A velocity triangle can now be drawn as in Figure 3 and some of the angles can be explained:

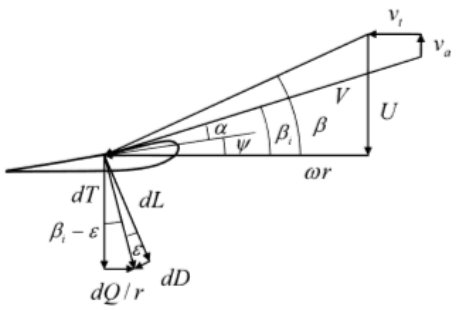

Figure 3: Schematic representation of the velocity and force triangles at a blade section (Melo, 2016).

β is the undisturbed aerodynamic pitch angle, the formula is: $\tan \beta = \frac{U}{\omega r} = \frac{1}{\lambda r^*}$,

where $r^* = \frac{r}{R}$ and λ is the tip speed ratio, defined as: $\lambda = \frac{\omega R}{U}$.

β_i is the induced aerodynamic pitch angle, it includes the effect of the axial and tangential induced velocities: $\tan\beta_i = \frac{U - v_a}{\omega r + v_t} = \frac{1 - v_a^*}{\lambda r^* + v_t^*}$,

where the induced velocities are made dimensionless: $v_{a,t}^* = \frac{v_{a,t}}{U}$.

α is the angle of attach, angle between the section chord line and the velocity projected on the blade cross section.

ψ is the blade pitch angle, geometrical angle between the blade chord line and the tangential direction. β_i and α are related to it by:

$$\psi = \beta_i - \alpha.$$

The total velocity V can be expressed in a dimensionless way with the formula:

$$V^* = \frac{V}{U} = \sqrt{(1 - v_a^*)^2 + (\lambda r^* + v_t^*)}.$$

Going back to Figure 3 it is now possible to mention the various components of the resulting force acting of the blade that appear:

L - Lift (per unit span). It is the projection of the resulting force in the direction perpendicular to $\vec{V}$;

D - Drag (per unit span). It is the projection of the resulting force in the same direction as $\vec{V}$;

T - Thrust. Projection of the resulting force in the axial direction;

Q/r - Circumferential force. Force that contributes to the torque in the tangential direction.

The most important dimensionless coefficients are:

$$C_L = \frac{L}{\frac{1}{2}\rho V^2 c} = \frac{2\Gamma}{Vc} = \frac{2\Gamma^*}{V^* c^*}, \qquad C_D = \frac{D}{\frac{1}{2}\rho V^2 c},$$

$$C_T = \frac{T}{\frac{1}{2}\rho U^2 \pi R^2}, \qquad C_P = \frac{P}{\frac{1}{2}\rho U^3 \pi R^2}.$$

The C_L and C_D data are usually given for a specific foil as function of the angle of attack and the Reynolds number Re defined as: $Re = \frac{Vc}{\nu}$ where ν is the kinematic viscosity of the fluid. They are usually obtained experimentally. The drag to lift coefficient ${}^{D}/_{L} = {}^{C_D}/_{C_L}$ is a very important parameter and is here represented with the letter ε.

Integrating along the span the infinitesimal thrust, considering the three blades it is possible to get the thrust coefficient as:

$$C_T = \frac{2Z}{\pi}\int_{r_h^*}^{1} (\lambda r^* + v_t^*)\,\Gamma^*(1 + \varepsilon\tan\beta_i)\,dr^*,$$

Same can be done for the power coefficient:

$$C_P = \frac{2Z\lambda}{\pi}\int_{r_h^*}^{1} \left(1 - v_a^*\right)\Gamma^*\left(1 - \frac{\varepsilon}{\tan\beta_i}\right) r^* dr^*.$$

Panel method

2.3 Potential flow problem

In the reference frame rotating with the turbine, the undisturbed inflow velocity is given by:

$$\overrightarrow{V_\infty}(x, r, \theta, t) = \overrightarrow{U_e}(x, r, \theta - \Omega t) - \vec{\Omega} \times \vec{x}, \tag{5}$$

where $\vec{x} = (x, y, z)$. In the reference frame rotating with the turbine, and under the assumption of irrotational flow the velocity field is described by a perturbation potential $\phi(x, y, z, t)$:

$$\vec{V}(x, y, z, t) = \vec{V}_\infty(x, y, z, t) + \nabla\phi(x, y, z, t). \tag{6}$$

The perturbation potential satisfies the Laplace equation:

$$\nabla^2\phi(x, y, z, t) = 0. \tag{7}$$

The boundary of the domain consists of the turbine blade surfaces S_B and the hub surface S_H. The perturbation potential must satisfy the following boundary conditions:

$$\nabla\phi \to 0, \text{ if } |\vec{x}| \to \infty \text{ and } x \neq +\infty, \tag{8}$$

at infinity, and a Neumann boundary condition:

$$\frac{\partial\phi}{\partial n} \equiv \vec{n} \cdot \nabla\phi = -\vec{n} \cdot \vec{V}_\infty \text{ on } S_B \text{ and } S_H, \tag{9}$$

where $\partial/\partial n$ denotes differentiation along the normal and $\vec{n}$ is the unit vector normal to the surface directed outward from the body. The boundary conditions on the wake surfaces S_W are the tangency of the fluid velocity on each side of the sheet:

$$\vec{V}_w \cdot \vec{n} = \vec{V}^+ \cdot \vec{n} = \vec{V}^- \cdot \vec{n} \text{ on } S_W, \tag{10}$$

and the continuity of the pressure across the vortex wake:

$$p^+ = p^- \text{ on } S_W, \tag{11}$$

where $\vec{V}_w$ is the velocity of the vortex sheet surface S_W, p is the pressure and the indices + and − denote the two sides of the vortex sheet, arbitrarily chosen on the upper side and lower side of the blade at the trailing edge, respectively. (Baltazar & Falcão de Campos, 2009)

2.4 Wake model

(Baltazar, Machado, & Falcão de Campos, 2011) The two boundary conditions on the wake are: the normal component of the fluid velocity is continuous and equal to the normal velocity of the wake surface , Eq. 10 and the pressure must be continuous across the wake surface, Eq. 11. The first condition, Eq. 10, implies that the vortex sheet

moves with the fluid. If $S_W(x,t) = 0$ represents the equation of the vortex sheet surface S_W, then:

$$\frac{\partial S_W}{\partial t} + \vec{V}^+ \cdot \nabla S_W = \frac{\partial S_W}{\partial t} + \vec{V}^- \cdot \nabla S_W = 0, \quad (12)$$

Outside of the vortex sheet the Bernoulli equation applies:

$$\frac{\partial \phi}{\partial t} + \frac{p}{\rho} + \frac{1}{2}\left|\vec{V}\right|^2 = \frac{p_\infty}{\rho} + \frac{1}{2}\left|\vec{V}_\infty\right|^2, \quad (13)$$

where p_∞ is the pressure of the undisturbed flow. Applying the Bernoulli equation at a given point on each side of the vortex sheet and subtracting the following expression is obtained:

$$\frac{\Delta p}{\rho} = -\frac{\partial(\Delta\phi)}{\partial t} - \frac{1}{2}\left(\left|\vec{V}^+\right|^2 - \left|\vec{V}^-\right|^2\right), \quad (14)$$

where $\Delta p = p^+ - p^-$ and $\Delta\phi = \phi^+ - \phi^-$ are the pressure and potential jump across the sheet, respectively.

From the boundary condition, Eq. 11, the pressure-jump is zero, we obtain from Eq. 14:

$$\frac{\partial(\Delta\phi)}{\partial t} + \vec{V}_m \cdot \nabla_S(\Delta\phi) = 0, \quad (15)$$

where $\vec{V}_m = \frac{1}{2}\left(\vec{V}^+ + \vec{V}^-\right)$ is the mean velocity and $\nabla_S(\Delta\phi) = \vec{V}^+ + \vec{V}^-$ is the surface gradient of the potential discontinuity, which is equal to the velocity discontinuity on the wake surface. Eq. 15 shows that the potential-jump remains constant following a fluid particle moving on the wake with the velocity $\vec{V}_m$. The Kutta condition states that the velocity must remain bounded at a sharp edge:

$$|\nabla\phi| < \infty. \quad (16)$$

2.5 Integral equation

Applying Green's second identity and using the Morino's formulation (Morino & Kuo, 1974), we obtain the integral representation of the perturbation potential at a point p of the body surface,

$$2\pi\phi(p,t) - \iint_{S_B \cup S_H}\left[G(p,q)\frac{\partial\phi}{\partial n_q} - \phi(q,t)\frac{\partial G}{\partial n_q}\right]dS = \iint_{S_W}\Delta\phi(q,t)\frac{\partial G}{\partial n_q}dS, \quad (17)$$

where $G(p,q) = -1/R(p,q)$, $R(p,q)$ is the distance between the field point p and the point q on the boundary $S = S_B \cup S_H \cup S_W$. The solution of Eq. 17 determines $\phi(q,t)$ on $S_B \cup S_H$, with $\partial\phi/\partial n_q$ known from Eq. 9. The Kutta condition, Eq. 16, yields the additional relationship between the dipole strength $\Delta\phi(q,t)$ in the wake and the surface dipole strength at the blade trailing edge and is applied in the form of pressure continuity at the trailing edge. (Baltazar & Falcão de Campos, 2009)

2.6 Velocity, pressure and forces

From the potential flow solution on the surface the velocity components can be calculated by surface differentiation. The pressure coefficient comes from Bernoulli equation and can be written as:

$$C_P = \frac{p - p_\infty}{1/2\rho{U_\infty}^2} = 1 - \left(\frac{|V|}{U_\infty}\right)^2,$$

where p_∞ is the pressure of the undisturbed flow.

The inviscid axial force T_i and the torque Q_i on the rotor are calculated from the pressure distribution on the blade surfaces:

$$T_i = \iint_{S_B} p n_x dS,$$

$$Q_i = \iint_{S_B} p(n_y z - n_z y)dS.$$

As in the lifting line theory, the quantities used to express the performance characteristics are the dimensionless power coefficient, axial force coefficient and the tip speed ratio. (Baltazar & Falcão de Campos, 2011)

3. IMPLEMENTATION

3.1 Numerical model

Lifting line discretization

As it is described in (Sousa, 2018), the lifting line is a finite vortex where the intensity is changing from hub to the tip. When translating this behaviour in terms of numerical model, the lifting line is discretized in 30 different smaller consecutive segments with constant value of circulation Γ_i, so the intensity of it will change by steps and not continuously. The point at the center of the segments are called control point r_i and the ones that bound them are called end point r_j. The control points are set closer to the tip because this is the region where the greatest gradients of circulations are expected. The distribution of the points follows a half-cosine distribution.

Induced velocities

The induced velocities due to the bound and the trailing vortices come from the Biot-Savart law and they can be written as linear combinations of the circulation as follows:

$$v_{a,t_i} = \sum_{j=1}^{M} C_{a,t_{ij}}\Gamma_j. \quad (18)$$

The $C_{a,t_{ij}}$ are the axial and tangential influence coefficients matrices ad they can be computed with 2 different methods.

When the wake is helicoidal because the alignment scheme is not applied, it is enough to compute the induced velocities at the lifting line, and this can be done through the analytical expressions of Lerbs (1952). When the wake is aligned with the fluid local velocity a numerical integration routine implemented in Melo (2016) can be used.

Optimization

The optimization procedure is the one that allows to find the optimum circulation distribution from which the

design can be done, choosing a lift coefficient and having the induced velocities distributions. The optimum distribution is the one that leads to the maximum power coefficient C_P for a given loading.

Classical optimization

As already explained in (Sousa, 2018), the optimum circulation distribution with this optimization is obtained when:

$$\frac{(\tan\beta_i)_i}{(\tan\beta)_i} = constant\ (l) \text{ for } i = 1, \dots, M. \quad (19)$$

This condition comes from the assumption that, with inviscid and uniform inflow, the loss of kinetic energy is minimized in the far wake where the induced velocities must follow the conditions $v_a \ll U$ and $v_t \ll \omega r$ (lightly loaded turbines).

The classical optimization system, after manipulating some of the equations is the following:

$$\sum_{j=1}^{M}\left(C_{a_{ij}} + \frac{\hat{l}}{\bar{r}_i}C_{t_{ij}}\right)\Gamma_j + l\lambda = 1 \text{ for } i = 1, \dots, M, \quad (20)$$

$$C_{T_0} = \frac{2Z}{\pi}\sum_{i=1}^{M}\left\{\left(\lambda\bar{r}_i + v_{t_i}\right)(1 + \varepsilon_i(\tan\beta_i)_i)\Delta r_i\Gamma_i\right\}, \quad (21)$$

where the M equations allow to find the circulation distribution and the imposed loading C_{T_0} expression allows to close to system in order to be able to get the constant l too. The value of C_{T_0} is changed multiple times until the maximum power coefficient C_P is obtained.

Discretization in the Panel code

As explained in (Baltazar & Falcão de Campos, 2011) for the numerical solution of the integral eq. 17 we discretise all the surfaces. The grid of the blade and hub and the initial grid on a rigid wake is generated by a ProPanel code.

The turbine blade surface is discretised in the spanwise radial direction by a set number of strips, extending chordwise from the blade leading edge to the trailing edge. Cosine spacing in the radial and chordwise directions is used.

The blade wake surface is discretised in the spanwise direction extending downstream from the trailing edge the corresponding strips on the turbine blade previously defined. The pitch both at the trailing edge and at the ultimate wake section is set as the aerodynamic pitch coming out from the design conducted through the lifting line code and the wake obtained is perfectly helicoidal.

Solution of the integral equation

The integral equation, Eq. 17, is solved by the collocation method with the element center point as collocation point. We assume a constant strength of the dipole and source distributions on each element. The influence coefficients are determined analytically using the formulations of (Morino & Kuo, 1974). To reduce the computation time, far field formulas are also used in the calculation of the influence coefficients. The linear system of equations is solved with a direct method (low triangular matrix and upper triangular matrix factorization).

The integral equation is solved through the in-house IST panel code called PROPAN. The output of the code is the wake geometry aligned with the local velocity, the circulation distribution, the thrust and power coefficients. Moreover, using a post processing code the pressure distribution in any blade section and the aerodynamic pitch at any radial or axial sections are found.

Kutta condition

The value of the dipole strength at the blade trailing edge $\Delta\phi$ is determined by the application of a Kutta condition. An iterative pressure Kutta condition is applied stating that the pressure is equal on the collocations points of the panels of the two sides adjacent to the trailing edge. At this point, the non-linear system of equations can be solved applying the method of Newton and Raphson (Skaflestad & Taylor, 2006), and the dipole strength at the blade trailing edge is found.

3.2 Convergence analysis

Numerical methods like the ones used in the lifting line theory and the panel method inevitably bring some errors with them: round off error, iterative error and discretization error.

The discussion on the errors is based on the panel method code, PROPAN. The circulation distribution, the optimum loading and the power coefficient are the variables computed for the analysis. Moreover, the geometry of the wake is continuously monitored through the software TecPlot in order to obtain the smoother geometry possible to be used in the lifting line code as input.

Wake alignment sections

The alignment in the panel method code was tested with different combinations of sections. It came out that the power and thrust coefficients variations get below 2% once the number of sections exceeds five (see Figure 4).

The combination of sections chosen expressed in axial dimensionless coordinates is {0, 0.05, 0.2, 1, 2}.

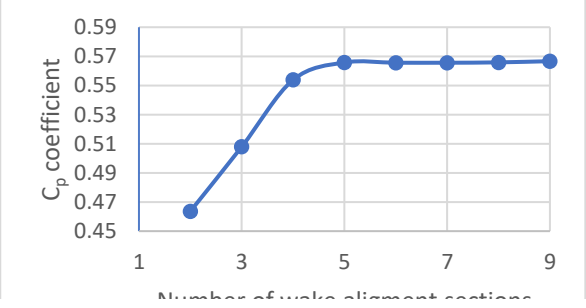

Figure 4: Convergence of the power coefficient changing the number of wake alignment sections.

Wake alignment iterations

The panel method code is let to run with different numbers of wake alignment iterations, going from 1 up to 10.

It was noticed that once the number of iterations exceeds 5 the differences in term of thrust and power coefficients get below 0.5% and for this reason it was considered good enough for our purposes (see Figure 5).

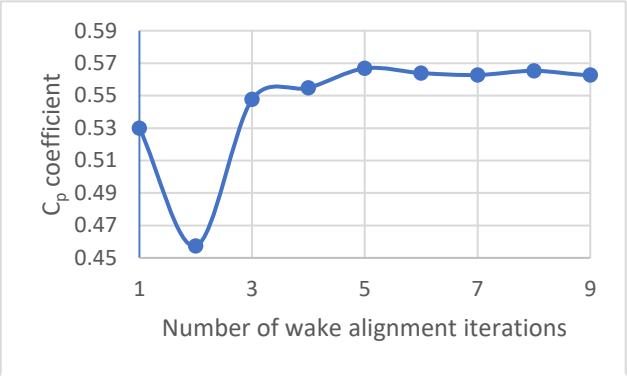

Figure 5: Convergence of the power coefficient changing the number of wake alignment iterations.

Number of panels per revolution

One last analysis was conducted using different number of panels per revolution of the wake. 40 as number of panels per revolution bring to a variation in the coefficients below 0.5% and for this reason it was considered a reasonable number of panels to consider (see Figure 6).

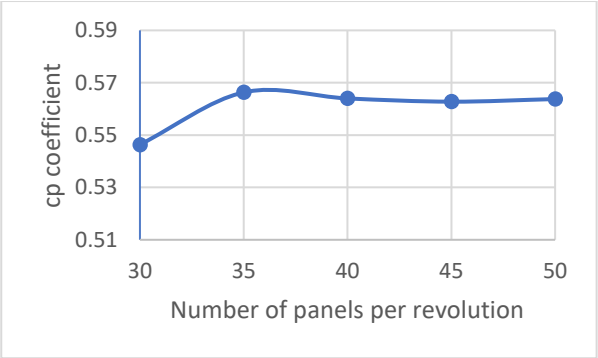

Figure 6: Convergence of the power coefficient changing the number of panels per revolution.

4. RESULTS

4.1 Issues in the computational procedure

During the computational procedure two main issues were encountered. The first problem encountered happens when the alignment of the wake is done using the PROPAN code. In fact, at around 60% of the blade length there are distortions in the wake obtained and to deal with this it was proposed to remove some of the strips for the computation of the induced velocities, adding a interpolation error that does not have any influence on the thrust and power coefficients calculations.

The second issue happens once the second and third designs iterations have to be done using the lifting line code. The original idea was to use the Lagrange multiplier method instead of the classical optimization but this was bringing to a weird circulation distribution, clearly wrong. The reason why the circulation obtained is distorted must be related with the transpose influence coefficients matrices. For the reason explained it was decided to use the classical optimization even in the second and third design iteration.

4.2 Inviscid results

In Figure 7 the circulation distributions for the three design iterations are shown and it is possible to notice that the differences between the second and the third design are very small, suggesting convergence behaviour.

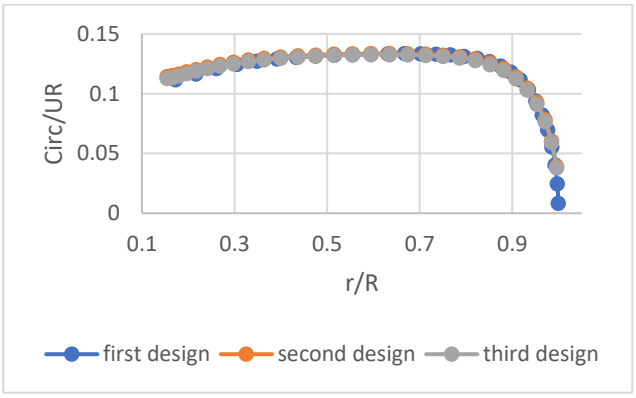

Figure 7: Circulation distribution for the three design iterations – inviscid case.

It is now possible to choose an angle of attack and a lift coefficient and the pitch and chord distributions can be found (Figure 8 and Figure 9). They both have the expected trend and the differences from the second to the third design are very small, in the order of about 2%, suggesting once again that the convergence in the design is being reached.

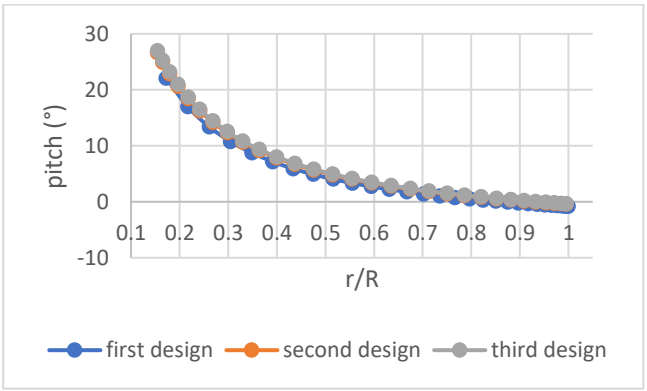

Figure 8: Pitch distribution for the three design iterations– inviscid case.

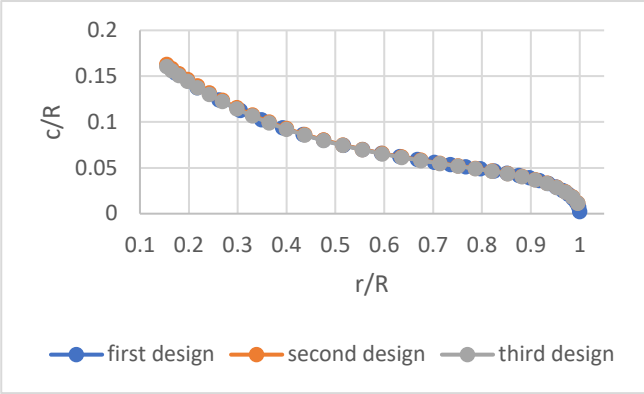

Figure 9: Chord distribution for the three design iterations – inviscid case.

In Table 1 it is shown the convergence of the power coefficient, keeping the thrust coefficient constant. It is possible to notice the increase of the power coefficient especially when going from the first design iteration to the second one, this leads to the conclusion that once the wake is aligned the power coefficient gets considerably higher, although the thrust coefficient keeps the same value.

Lifting line code	**ProPan code**
C_T = 0.804; C_P = 0.520	C_T = 0.808; C_P = 0.564
C_T = 0.804; C_P = 0.560	C_T = 0.771; C_P = 0.555
C_T = 0.804; C_P = 0.562	

Table 1: Convergence of thrust and power coefficients – inviscid case.

The wakes could be drawn and it is possible to notice that with the first design the wake is perfectly helicoidal (Figure 10) and then in the second (Figure 11) and in the third design (Figure 12) the wake is aligned with the local velocity of the flow because the wake obtained though the panel method code is used as input in the next lifting line design iteration.

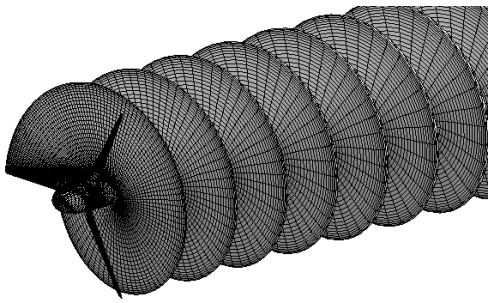

Figure 10: Helycoidal wake – inviscid case.

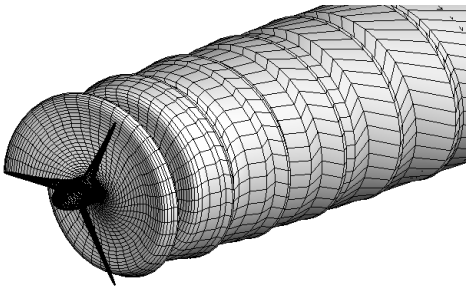

Figure 11: First aligned wake – inviscid case.

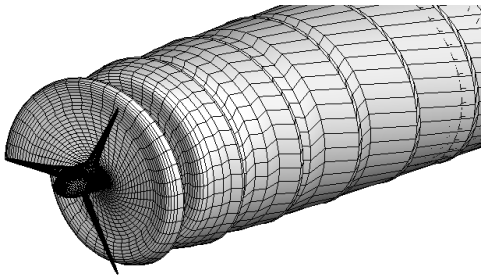

Figure 12: Second aligned wake – inviscid case.

To prove the folding behaviour from a more analytical point of view, a post processing code that uses the wake as input and give the pitch distribution as output is used. The distribution of the pitch at the lifting line is obtained through the lifting line optimization and it is constant since the optimization procedure used is the classical one. When looking at the distributions at different axial sections (Figure 13) it is possible to see that the pitch tends to increase approaching the tip, unlike Sousa's results where in the sections close to the rotor plane the pitch was decreasing close to the tip. The yellow line in the graph, unlike the orange and grey ones, shows that the behaviour of the pitch tends to be constant from 15% to 80% of the blade length at the alignment section $^{x}/_{R} = 1$.

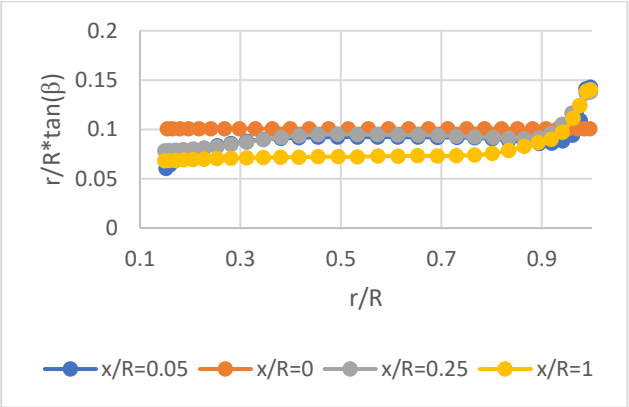

Figure 13: Radial distribution of the pitch – inviscid case.

It is interesting to show not only the radial pitch distribution at different axial sections but also how the pitch at a given radial coordinate evolves going downstream, this is represented in Figure 14. Although some initial fluctuations from the trailing edge to $^{x}/_{R} =$

0.8 it is possible to conclude that the wake tries to keep a constant value of the pitch for each radial position, this makes total sense because we are moving in the far wake region.

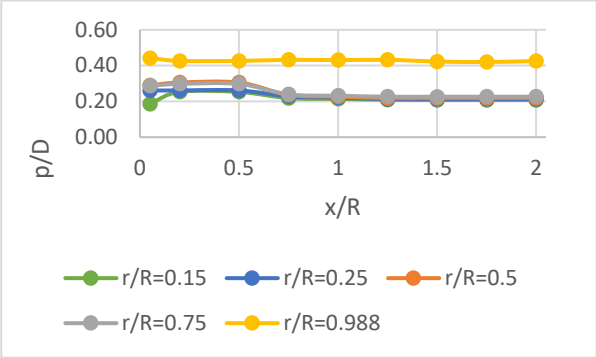

Figure 14: Axial distribution of the pitch.

The discussion of the results for the inviscid case finally ends showing the pressure distribution at 3 different radial sections (Figure 15). The pressure varies in the chordwise direction as shown, the regions of lower and upper pression are easily recognizable and the shape of the graphs obtained is fully coherent with the ones coming from the work of (Hogan, 2010).

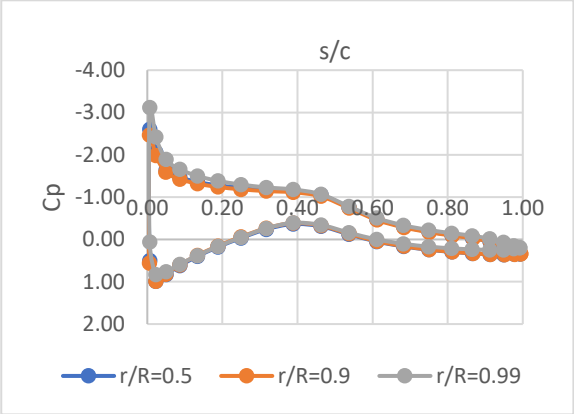

Figure 15: Pressure distribution at three different radial sections.

4.3 *Viscous results ($\varepsilon = 0.01$)*

The circulation distributions of the second and third design are very similar, as it happens in the inviscid situation. It falls drastically down to zero after 80% of the blade length and the classical optimization is used.

The second and third design graphs of blade pitch and chord show high similarity again, as it happens in the inviscid case and the explanation of the trends is exactly the same.

In the same way as done for the inviscid case procedure, the power coefficient is optimized in the first design and the corresponding thrust coefficient is used from that moment on when the lifting Line design occurs. The PROPAN code analysing the turbine gives as output the thrust and power coefficients that are not interesting for us since the PROPAN calculation work in such a way that is not able to take into account the viscous effects. In order to correct those coefficients the drag effects must be taken into account and a post processing code in which the distribution of drag and lift is provided as input is used: the thrust coefficient does not really change but the power coefficient does and it gets lower, approaching the one found with lifting line optimization. In fact, in the second cycle the power coefficient is 0.513 and the one found through viscous corrections is 0.529. Again, the convergence in terms of power coefficient is achieved: when the third lifting line optimization is made the power coefficient is 0.519, value very close to the second design power coefficient (0.513). All the values of thrust and power coefficients are reported in Table 2.

Lifting line code	**PROPAN code**	**PROPAN code (viscous effects)**
$C_T = 0.795$ **$C_P = 0.483$**	$C_T = 0.847$ $C_P = 0.575$	$C_T = 0.852$ $C_P = 0.532$
$C_T = 0.795$ **$C_P = 0.513$**	$C_T = 0.815$ $C_P = 0.570$	$C_T = 0.819$ $C_P = 0.529$
$C_T = 0.795$ **$C_P = 0.519$**		

Table 2: Thrust and power coefficients – viscous case.

The first wake is perfectly helicoidal, as it is not aligned and the pitch is uniform everywhere and equal to the lifting line one. The second and the third wakes (Figure 16) folds in the downstream direction at any axial alignment section as expected. In this case it is not possible to compare the wake geometries with Sousa's results because he did not make any studies on the wake geometry with the viscous flow assumption.

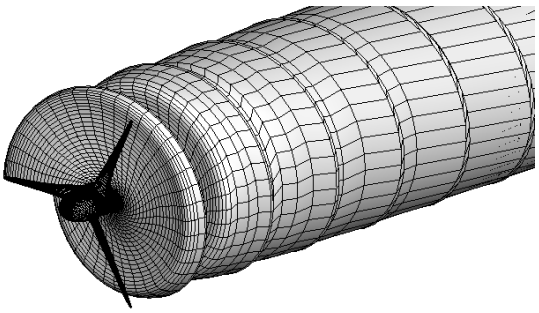

Figure 16: Second aligned wake – viscous case.

Looking at the pitch distributions at many different axial sections (Figure 17) it is possible to confirm the folding behaviour of the wake, in fact the pitch keeps its value constant until 80% of the blade length and then it increases, this does not happen at the lifting line where the pitch is constant because of the fact that the classical optimization is used.

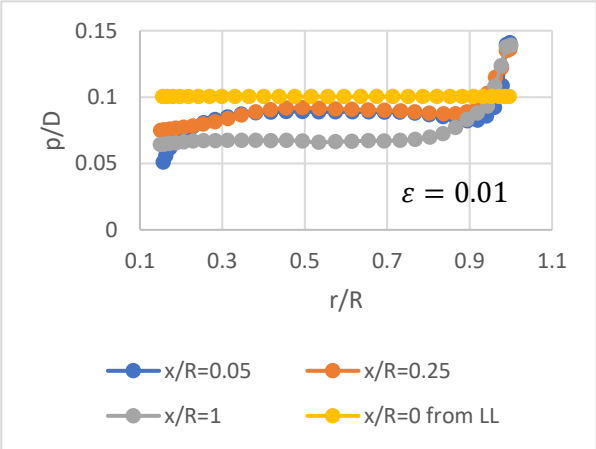

Figure 17: Pitch for given radial coordinates – viscous case.

The pitch along the downstream direction shows again that after an initial phase in which the values fluctuate, after the coordinate to $^{x}/_{R} = 0.7$ the pitch at each radial coordinate is almost constant, this happens because the transition wake is probably over and the pitch tries to behave as constant.

The pressure distribution has a similar shape to the one shown in the inviscid situation therefore it was decided not to represent it here.

4.4 Comparison of the cases

It is possible to conclude that the thrust and power coefficients are lower in the case of viscous flow, where the lift to drag coefficient is equal to 0.01 (see Table 3). This was predictable from the power coefficient formula and it makes sense that the wind power extracted by the rotor is lower for the viscous case since the losses related to the viscosity of the flow are not neglected anymore.

Inviscid	**Viscous ($\varepsilon = 0.01$)**
C_T = 0.804	C_T = 0.795
C_P = 0.562	C_P = 0.519

Table 3: Thrust and power coefficients for the inviscid and viscous cases

In terms of circulation distribution, the highest difference for a given radial coordinate is around 1%, a similar result was found by (Chattot, 2003), in fact there it is stated that viscous correction only causes a minor effect on the optimum geometry of the blade. The same happens with the blade pitch angle distribution.

The situation is slightly different in the case of the chord distribution (Figure 18), in fact the graphs are quite different, the variation of the two graphs is around 11% at every radial coordinate and the reason why this happens is related to the choice of the lift coefficient. The lift coefficient in the inviscid case is 0.94 while in the viscous one is 0.84 and this brings to a higher chord in the viscous case.

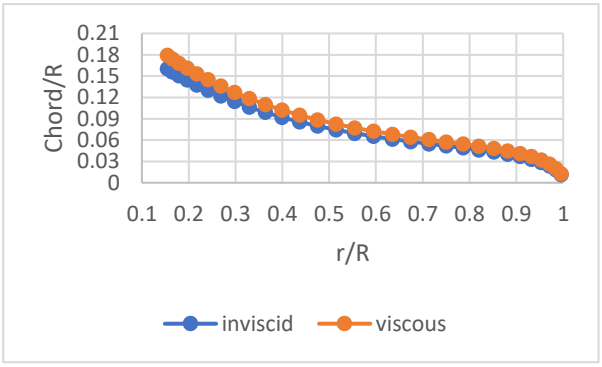

Figure 18: Comparison of the design chord between the inviscid and viscous flow.

5. CONCLUSIONS

In this work the lifting line optimization procedure by (Sousa, 2018) is combined with a code able to analyse the rotor through the panel method code. The inviscid design of the blades is done starting from the optimum circulation distribution, choosing a lift coefficient and performing the blade design. The analysis of the rotor with specific air inflow conditions is carried out and a wake geometry aligned with the local fluid velocity is obtained that can be used as input in a second iteration cycle in which the lifting line optimization is done based on the wake geometry obtained with the panel method. The entire cycle may be repeated several times. It was noticed in fact, that after three lifting line optimizations the power coefficient shows convergence behaviour so it is possible to stop the iteration lifting line code – panel code. A convergence analysis on the panel code was conducted too, to show the effect of the alignment sections, the number of iterations and the number of panels per revolution of the wake.

It was shown that using the combination of lifting line and panel method a physically acceptable result was obtained. With the wake alignment procedure used in this study, the pitch distribution has the correct trend very close to the rotor plane $(^{x}/_{R} = 0.05)$. Naturally, in all the other alignment sections downstream the behaviour of the pitch distribution is the right one too with the wake folding in the downstream direction.

The viscous effect was investigated doing all the procedure above explained setting a drag to lift ratio equal to 0.01. Again, the wake geometry obtained is physically acceptable but when it comes to compare the design with the inviscid one the only remarkable difference lies on the chord distribution, and this comes from the choice of the lift coefficient that in this case must be inevitably lower, due to the viscous effects that are playing a fundamental role.

In terms of future work there are many suggestions and improvements that could be done starting from the model

shown. First of all, we were not able to use the Lagrange multiplier optimization in the lifting line and this would have set less constraints to the optimization problem. More efforts have to be put on the understanding of the weird wake geometries obtained through the panel method code using specific combinations of alignment sections and without removing some of the radial strips. Also, some parametric studies would show the effects of different tip speed ratios and drag to lift coefficients in terms of thrust and power coefficient and wake geometry too. It would be interesting to see if going ahead with the iterations lifting line code – panel code the power coefficient would continuously converge and based on that the design would be done starting from the corresponding circulation distribution. Moreover, the design of the blade could be done in such a more realistic way in which the chord at the tip does not go to zero and the computation of the radial induced velocities could bring to the expansion of the wake. Finally, different choices of the lift coefficient and angle of attacks could show how the design of the blades would change.

REFERENCES

Anderson, J. D. (2001). Fundamental of aerodynamics. *McGraw-Hill*, Boston.

Baltazar, J., & Falcão de Campos, J. A. C. (2009). Unsteady Analysis of a Horizontal Axis Marine Current Turbine in Yawed Inflow Conditions With a Panel Method. *First International Symposium on Marine Propulsors*, (June), 9.

Baltazar, J., & Falcão de Campos, J. A. C. (2011). Hydrodynamic Analysis of a Horizontal Axis Marine Current Turbine With a Boundary Element Method. *Journal of Offshore Mechanics and Arctic Engineering*, *133*(4), 041304. https://doi.org/10.1115/1.4003387

Baltazar, J., Falcão de Campos, J. A. C., & Bosschers, J. (2012). Open-Water Thrust and Torque Predictions of a Ducted Propeller System with a Panel Method. *International Journal of Rotating Machinery*, *2012*, 1–11. https://doi.org/10.1155/2012/474785

Baltazar, J., Machado, J., & Falca˜o de Campos, J. A. C. (2011). Hydrodynamic Design and Analysis of Horizontal Axis Marine Current Turbines With Lifting Line and Panel Methods (pp. 453–465). ASMEDC. Retrieved from https://asmedigitalcollection.asme.org/OMAE/proceedings/OMAE2011/44373/453/350993

Caldeira, J. M. R. (2014). Análise de um Modelo de Perda para o Cálculo Aerodinâmico da Turbina Eólica de Eixo Horizontal NREL / NWTC com o Método da Linha Sustentadora - *MSc Thesis in Mechanical Engineering*. Instituto Superior Tecnico.

Chattot, J.-J. (2003). Optimization of Wind Turbines Using Helicoidal Vortex Model. *Journal of Solar Energy Engineering*, *125*(4), 418. https://doi.org/10.1115/1.1621675

Duarte, R. S., & Falcão de Campos, J. A. C. (1997). Numerical model of propeller vortex wakes for calculation of induced velocities, (1989).

Erickson, L. (1990). NASA Technical Paper Panel Methods-An Introduction. Moffett Field, California.

Falcão de Campos, J. A. C. (2007). Hydrodynamic Power Optimization of a Horizontal Axis Marine Current Turbine with Lifting Line Theory. In *Proceedings of the Seventeenth (2017) International Offshore and Polar Engineering Conference* (pp. 307–313). Lisbon, Portugal.

Hogan, F. (2010). Análise do Desempenho Aerodinâmico da turbina Eólica NREL com um Método de Elementos de Fronteira - *MSc Thesis in Mechanical Engineering*. Instituto Superior Tecnico.

Lanchester, F. W. (1907). Aerodynamics. *Archibald Constable & Co. LTD*.

Lerbs, H. W. (1952). Moderately Loaded Propellers with a Finite Number of Blades and an Arbitrary Distribution of Circulation. *Transactions of the Society of Naval Architects and Marine Engineer*, *60*(1952), 73–123.

Machado, J. L. (2010). Projecto hidrodinâmico de turbinas de corrente marítima de eixo horizontal com o modelo da linha sustentadora - *MSc Thesis in Mechanical Engineering*. Instituto Superior Tecnico.

Melo, D. B. (2016). Analysis of Horizontal Axis Wind Turbines with Lifting Line Theory - *MSc Thesis in Mechanical Engineering*. Insituto Superior Tecnico.

Morino, L., & Kuo, C. . (1974). Subsonic Potential Aerodynamics for Complex Configurations : A General Theory. *AIAA Journal*, *12*(2), 191–197. https://doi.org/10.2514/3.49191

Skaflestad, B., & Taylor, M. (2006). Newton's method for systems of non-linear equations. Trondheim, Norway.

Sousa, G. (2018). Aerodynamic Optimization of Horizontal Axis Wind Turbines Using the Lifting Line Theory - *MSc Thesis in Mechanical Engineering*. Instituto Superior Tecnico.